Effect of water content on microwave dielectric properties of building materials

Romain Damez, Philippe Artillan, Arthur Hellouin de Menibus, Cédric Bermond, Pascal Xavier

Effect of water content on microwave dielectric properties of building materials

Romain Damez[a], Philippe Artillan [a], Arthur Hellouin de Menibus[b], Cédric Bermond [a], Pascal Xavier[a]

[a] Univ. Grenoble Alpes, Univ. Savoie Mont Blanc, CNRS, Grenoble INP*, IMEP-LAHC, 38000 Grenoble, France

* Institute of Engineering Univ. Grenoble Alpes

[b] Ecopertica, Hôtel Buissonnet, 61340 Perche en Nocé & Association des Chanvriers en Circuits Courts, France

Corresponding author: Philippe Artillan – philippe.artillan@univ-smb.fr

Abstract

This paper presents measurement results of the complex dielectric permittivity depending on the humidity for a range of materials used in buildings. It covers a whole range from light to heavy materials with different hygroscopic properties and with a special focus on green building materials. Two specific adjustable stripline test devices of different lengths have been designed and used to perform the extractions of the permittivity from S-parameters measurements using the two transmission lines method. The study covers a frequency band extending from 500 MHz to 2.5 GHz and is carried out on dry, ambient and wet conditioned samples. The main trends are physically discussed, and phenomenological explanations based on the impedance matching and the water absorption among others are proposed for the observed behaviors. The use of the obtained data is illustrated through the extraction of the electromagnetic behavior of a realistic wall.

Preprint submitted to Journal of Construction and Building Materials

Keywords: Electromagnetic propagation, Absorbing media, Transmission line measurements, Permittivity, Green buildings, Dielectric constant, Losses, Moisture, Water content, Humidity.

2010 MSC: 00-01,99-00

1. Introduction

Constructors have shown increasing interest in knowing the behavior of the materials they use regarding electromagnetic waves, in addition to their mechanical, thermal and acoustic properties. The properties of materials under outdoor conditions vary as a function of the Gravimetric Water Content (GWC). The GWC is directly related to the ambient Relative Humidity (RH) by the sorption curve specific to the material. As a consequence, the RH greatly influences the electromagnetic behavior over a wide frequency range of porous materials such as clay [1], concrete [2-4], soils [5], wood [6] or wheat [7]. It is therefore of interest to look in more detail how the RH influences the electromagnetic behavior of building materials at a specific frequency range for two reasons. First, questions were raised about telecommunication signal transmission in buildings made of large walls. It is asked to clear out how different materials behave and why, depending among others on their density and their ability to interact with water. Secondly, based on on-site dielectric measurements and an inverse problem approach, it would thus be possible to estimate the GWC for an existing structure by measuring its dielectric properties.

The purpose of the study presented here is therefore to characterize the microwave dielectric properties of some building materials from 500 MHz to 2.5 GHz, in particular those used in the green building sector, and to observe their evolution as a function of relative humidity (RH). Previous works deal with insulating green building materials with quite high variability [8], and this study aims at addressing a large batch of materials conditioned through the same protocol in order to provide additional results.

After describing the methodology used to measure and extract the dielectric permittivity, the materials under test are presented and their conditioning is discussed

in section 2. Section 3 presents the permittivity extraction results and discusses their uncertainties. Finally, section 4 gives a turnkey method and provides computation examples to simulate the electromagnetic response of any multilayer wall made of building materials.

2. Dielectric permittivity characterization methodology

2.1 Extraction method

A strong interest for measuring the complex permittivity of materials has been shown for decades. In this purpose, several methods have been proposed. The capacitive method consists in measuring the capacitance of a sample placed between two metallic plates [9]. Although this method provides a good accuracy, the thicker the samples, the larger they are required to be to avoid edge effects. Furthermore, this method is only suitable for frequencies below several tens of MHz.

Many resonant methods have also been proposed as reviewed in [10], in particular, the resonant cavity method [11], dielectric resonators [12] or printed ring resonators [13-14]. The resonant frequency varies depending on the material loading the device. Although good sensitivity to losses can generally be achieved by such methods, the main drawback is that a unique frequency point is provided for a specific test device.

Thereafter, characterization in free space consists in placing a sample of a certain thickness between two beaming elements such as antennas [15-17]. Depending on its dielectric permittivity, the sample would reflect, dampen and transmit parts of the incident wave. This information is accessible on large frequency bands and can be retrieved from S-parameters, provided the lengths of the setup (thickness of the sample, distance to the antennas) are known with great accuracy. Large samples are required to avoid edge effects due to the beaming aperture of the antennas.

Wide band coaxial probe methods can also be cited [18-19]. Probe(s) are placed upon the surface of a sample, and the permittivity can be extracted by measuring the

reflection or the transmission coefficient. This method is still very sensitive to the quality of the contact due to the roughness of the sample.

Finally, it is possible to extract the dielectric permittivity of materials by a frequency or time measurement of a loaded transmission line [20]. The material is filling the gap between the two conductors and tweaks the propagation constant of the transmission line.

Given the geometrical characteristics of the samples of this study and the limitations of the different setups, it has been chosen to use the loaded transmission lines method with a stripline structure, as used in [21]. This structure, composed of a center conductor located between two ground planes, in a quasi-transverse electromagnetic (quasi-TEM) configuration, allows practical easiness and simple numeric extraction from measured S-parameters that is described in part 2.2 of this section.

2.2 *Setup and extraction scheme*

In order to measure the complex dielectric permittivity of some building materials of interest over a large range of frequencies, two aluminum stripline test devices of length 8 cm and 10 cm have been built (Fig. 1). The test devices allow measurements with and without Material Under test (MUT), for various thicknesses of MUT.

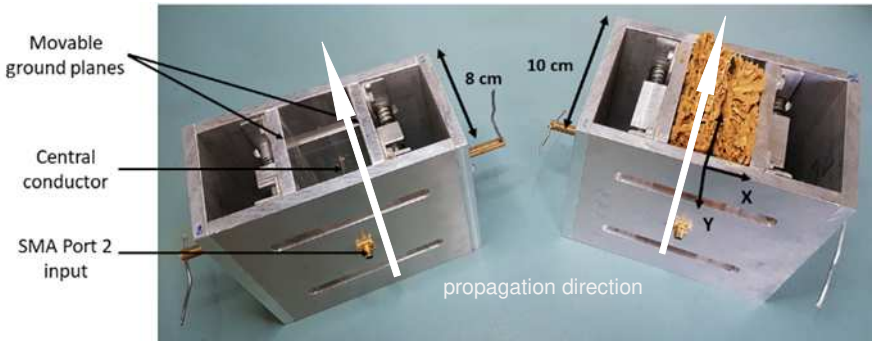

Fig. 1. Photography of the test devices used for the extraction of the complex relative permittivity of some Material Under test (MUT). The left transmission line is 8 cm length and not loaded. The right transmission line is 10 cm length and is loaded with hemp clay pieces. SubMiniature version A connectors (SMA) have been used.

Four measurements of scattering parameters (S-parameters) were performed for each extraction of $\bar{\epsilon}_{rMUT}$, as shown in Fig. 2: (a) the short transmission line loaded with air, (b) the long transmission line loaded with air, (c) the short transmission line loaded with MUT, and (d) the long transmission line loaded with MUT.

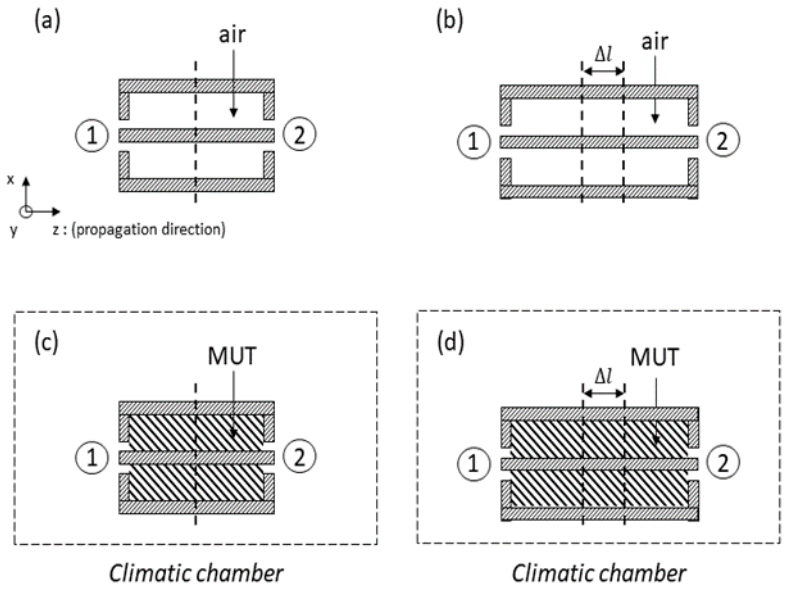

Fig. 2. Stripline test devices: measurement setup.

The extraction methodology is based on the property of transmission lines with homogeneous dielectric material of which electric field cartography remains unchanged whatever the dielectric permittivity. For a stripline structure filled with homogeneous dielectric material, the electric field map is independent of the complex relative permittivity $\bar{\epsilon}_r$. The capacitance per unit length C and conductance per unit

length G of such a structure can then be expressed as a function of $\bar{\epsilon}_r$ and a geometrical factor $\mathcal{G}$ which is independent of $\bar{\epsilon}_r$:

$$(G + j\omega C) = j\omega\mathcal{G}\epsilon_0\bar{\epsilon}_r \quad (1)$$

Considering equation (1), one can express the propagation constant γ_{MUT} of a stripline structure loaded with some material under test (MUT) of unknown relative permittivity $\bar{\epsilon}_{rMUT}$:

$$\gamma_{MUT} = \sqrt{j\omega\mathcal{G}\epsilon_0\bar{\epsilon}_{rMUT}(R + j\omega L)} \quad (2)$$

where L is the inductance per unit length and R resistance per unit length.

The propagation constant γ_{AIR} of the same stripline structure filled with air of relative permittivity $\bar{\epsilon}_{rAIR} = 1$ can also be expressed as:

$$\gamma_{AIR} = \sqrt{j\omega\mathcal{G}\epsilon_0(R + j\omega L)} \quad (3)$$

Dividing (2) by (3) and taking the square of the result leads to the formula used for the extraction of $\bar{\epsilon}_{rMUT}$:

$$\bar{\epsilon}_{rMUT} = \left(\gamma_{MUT}/\gamma_{AIR}\right)^2 \quad (4)$$

All measurements were performed at ambient temperature with the Vector Network Analyzer Keysight N9914A from 500 MHz to 2.5 GHz (401 points). The used power is -5 dBm and a 100 Hz IF filter bandwidth is applied. The MUT were placed in a climatic chamber to control the RH and consequently the GWC.

The propagation constants γ_{MUT} and γ_{AIR} have been computed from S-parameters with high accuracy using the auto-calibrated method presented in [22]. This method only requires the measurement of two transmission lines of different lengths for the determination of one propagation constant. The length difference $\Delta l = 2cm$ between the two transmission lines has been chosen to avoid the 180° phase angle difference at the maximum frequency of 2.5 GHz for relative permittivity of 4, which corresponds to the maximum permittivity encountered for the materials of interest, and is then the worst case. This dimensioning allows the maximum accessible sensitivity for the extraction method as fully developed in [23]. This differential extraction scheme is extremely robust as only the length difference Δl between the two transmission lines must be known, while numerous unknown terms simplify in the calculus of $\bar{\epsilon}_{rMUT}$:

150 geometrical factor $\mathcal{G}$ (electric field map), lineic resistance R and lineic inductance L (conductors effects). Furthermore, no preliminary calibration is required, in the same manner as for the well-known Thru-Reflect-Line (TRL) calibration technique.

2.3 Preparation and conditioning of sample materials

Ten samples of thicknesses varying between 1 cm and 2 cm were studied in this
155 experiment: cement concrete, hemp-clay mixture, clayed earth and sand mixture prepared by a professional builder, wood wool, wood fiber, rock wool and Fermacell® panels, woodchip agglomerates referenced as OSB3 and MFP in trade, and cork (see fig. 3). The choice was made to cover a large and representative diversity of the materials used in the eco-construction sector.

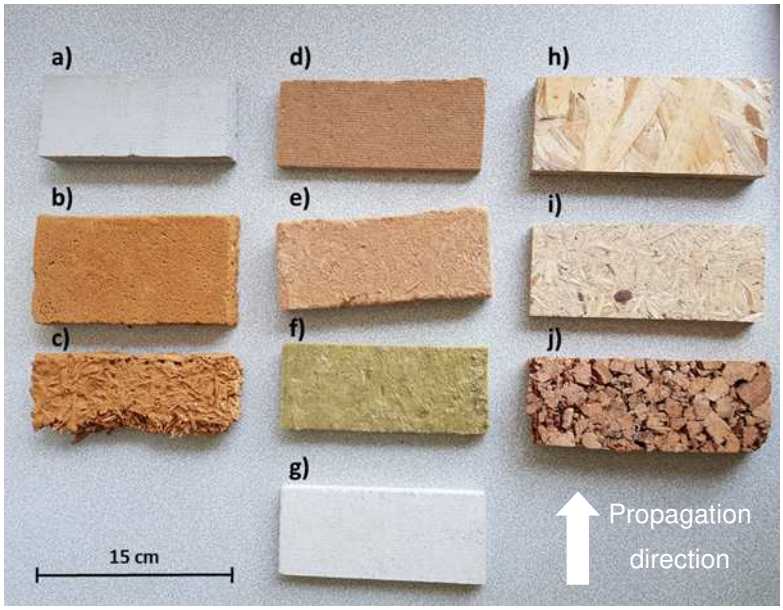

160

Fig. 3. Photography of the eco-materials. a) Cement concrete ; b) Clayed earth + sand ; c) Hemp-clay ; d) Dense wood fiber ; e) Light wood fiber ; f) Rock wool ; g) Gypsum-fibers Fermacell® ; h) Wood panel OSB3 ; i) Wood panel MFP ; j) Cork.

The hemp-clay sample is representative of light earth thermal insulation. The clayed earth is the natural earth clay 1 studied in [24], with 37 % of clay and with normal activity (the activity is related to the cohesion level of the clayed earth). Table 1 gives more details on the composition and the building process of the studied materials.

A sample of PolyVinyl Chloride (PVC) was also studied as a reference material in order to validate the measurement method.

The samples were then conditioned in order to reach ambiences characterized by determined RH so that the GWC of the materials is modified. Three different ambiences of RH were established with 5 % (dry), 40 % (ambient) and 80 % (wet), allowing to study the dielectric properties of the materials under various realistic conditions. RH here refers to the ratio between the partial pressure of water vapor and the saturation vapor pressure. For the ambient and wet ambiences, the samples were placed in a climatic chamber during at least 6 days. Starting from the 5th day, the mass of the sample was measured, and it was assumed that the balance was reached since the weight was not varying by more than 0.1 % over the following 24 hours. For the dry ambience, the samples were heated at 70°C in an oven by cycles of 3 hours. The sample masses were controlled between each cycle and as many cycles as necessary were conducted until the measured mass was stabilized (less than 0.1 % of relative variation). This latter process brings the dry mass of each material and its water content over the three ambiences is then accessible by mass monitoring.

3. Dielectric permittivity extraction results

3.1 Dielectric permittivity measured values

Extraction traces over the frequency band at the three RH values have been plotted for all materials presented in 2.3. As examples, the extraction traces are given in Fig. 4 for light wood fiber (a) and wood panel OSB3 (b).

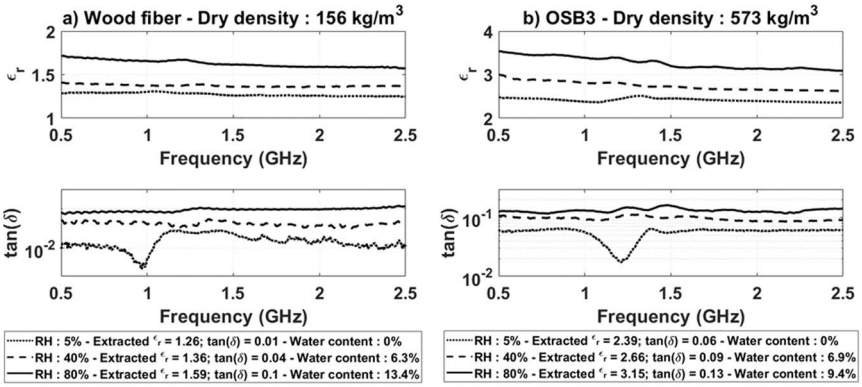

Fig. 4. Extraction traces at the three RH rates for (a) light wood fiber and (b) wood panel OSB3.

The measurements carried out with the transmission lines have shown almost constant extracted parameters over the frequency band of study for all materials. In order to explore the data on the ten materials at three different RH each, a single value of relative permittivity and loss tangent has been chosen for each frequency extraction using a function that identifies the most commonly encountered (the position of the peak of the probability density function) value over the frequency band. Furthermore, to take the uncertainties presented in 3.3 into account, the loss tangent was set to 1×10^{-2} if it was estimated below this value.

The extractions of the dielectric permittivity for all the materials are given in Table 1 and represented in Fig. 5.

Material	Description	Dry density (kg/m³)	RH (%)	GWC (%)	ε_r	$\tan\delta$ ($\times 10^{-2}$)
Light wood fiber (wool)	20 mm thermal insulation panel	156	5	0.0	1.26	1
			40	6.3	1.36	4
			80	13.4	1.59	10
Rock wool	15 mm thermal insulation panel Rocksol® (Rockwool)	195	5	0.0	1.09	2
			40	0.6	1.15	1
			80	1.1	1.16	1
Dense wood fiber	10 mm thermal insulation panel Isorel® (Steico)	247	5	0.0	1.17	1
			40	8.0	1.30	4
			80	11.6	1.55	7
Cork	20 mm pumiced cork panel (Alsacork)	248	5	0.0	1.12	1
			40	6.2	1.20	2
			80	8.1	1.37	3
Hemp-clay	20 mm hemp shiv (90 kg/m³)	424	5	0.0	1.35	1

	Hemp/clay ratio: 0.55		40	5.9	1.55	7
			80	8.9	1.73	11
Wood panel OSB3	15 mm "Oriented Stand Board 3"	573	5	0.0	2.39	6
			40	6.9	2.66	9
			80	9.4	3.15	13
Wood panel MFP	12 mm Multifunctional Plate Board Pfleiderer MFP® premium board P5	687	5	0.0	1.90	3
			40	6.8	2.19	8
			80	10.8	2.85	12
Gypsum-fibers	10 mm board made of gypsum reinforced by cellulose (Fermacell®)	1274	5	0.0	3.35	1
			40	1.2	3.50	3
			80	2.2	3.73	3
Clayed earth + sand	20 mm mix validated by the builder 1 volume of clayed earth + 3 volumes of 0/2 sand	1825	5	0.0	2.29	3
			40	1.1	2.69	5
			80	2.0	2.94	6
Cement concrete	20 mm mix 1 volume of Calcia i.pro Technocem 3 volumes of 0/2 sand	2088	5	0.0	3.41	1
			40	0.8	3.65	1
			80	1.4	3.84	2
PVC	20 mm Kömadur (Polydis)	1445	40	0.0	2.97	2

Table 1. Studied materials and measured the complex dielectric permittivity.

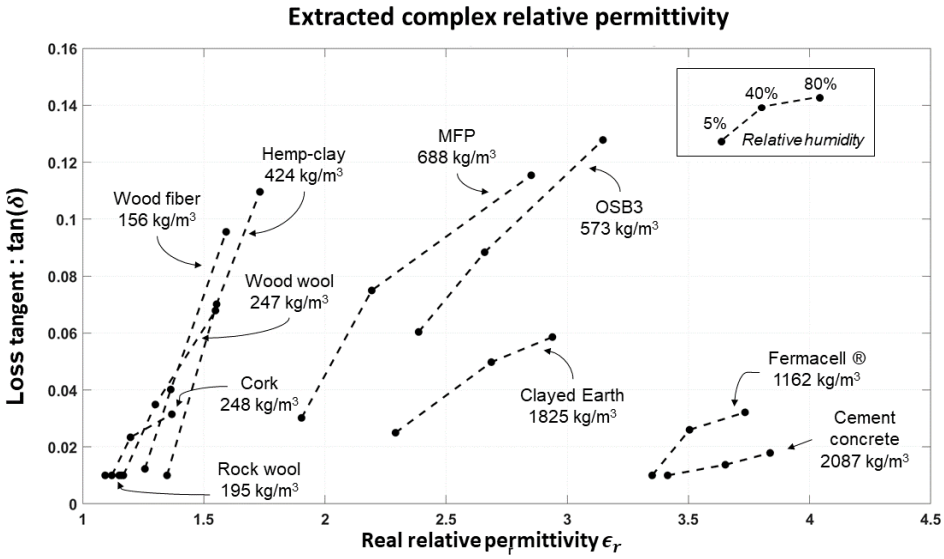

Fig. 5. Real relative permittivity and loss tangent of tested materials under various relative humidity conditions.

3.2 *Discussion*

Looking at fixed dry or ambient state, it is clear that the higher the density of the materials, the higher the relative permittivity, which is in compliance with the results of [25]. The very light materials, such as hemp-clay, rock wool, light wood fiber and cork have their real relative permittivity close to the unit and a very low loss tangent. This is explained by their high porosity as they are mostly filled with air.

For cellulosic materials, such as light wood fiber, dense wood fiber and cork, the general tendency is that both the real relative permittivity and the loss tangent increase with RH, that is to say with the GWC. The order of magnitude of the variation of the relative permittivity from the dry to the wet conditioning is about half a unit, while the loss tangent can vary up to one order of magnitude [26].

As the measured GWC are below 10 %, we can assume that most part of the water retained in the materials is bound water rather than free water [27]. In a wet ambience, water molecules link to the material and the resulting material is thus a mixture between the bulk material and water, both of which having their own impact on the global dielectric response. Bound water is known for having very high real relative permittivity and loss tangent, around $(17.3, 5.2 \times 10^{-1})$ at 1 GHz [28]. Bound water is then responsible for the rises of the dielectric parameters of the studied materials.

The evolution of the dielectric loss from the dry to the wet state seems to be correlated with the water content variations. Indeed, with the highest water contents in terms of mass, the woods and the hemp clay present greater loss tangents in wet state than any other material.

We can also make comparisons between materials presenting the same macroscopic structure or the same behavior.

First, the loss tangent of light wood fiber and dense wood fiber increase by 6×10^{-2} and 9×10^{-2} respectively whereas rock wool's dielectric properties almost do not vary with RH. In fact, as organic materials, the wooden compounds are much more able to soak water up (28.7 and 20.9 kg/m^3 – more than 11 % in mass) than rock wool which is mineral (2.2 kg/m^3 – 1.1 %).

Second, the wood particles panels have their relative permittivity comprised between 2.28 and 2.82 at ambient state (40 % RH). The obtained values are consistent with the manufacturing variability and the composition (cellulose, hemicellulose, lignin, air and moisture) of wood particles panels, as previously published in studies [29-31].

Finally, cement concrete and gypsum-fibers (Fermacell®) have a similar relative permittivity increasing from 3 to 4 with RH, in spite of a high density discrepancy, Fermacell® being much less dense because of the light cellulosic fibers incorporated in the gypsum. Gypsum's relative permittivity was measured at 6.5 at 750 MHz in [32]. The dielectric properties of gypsum and cellulose explain why Fermacell®'s permittivity is comprised between 3 and 4. On the other hand, the cement used in the studied sample is mainly composed of limestone, the relative permittivity of which was measured in [33] around 7 at 100 MHz at dry state. The permittivity of sand is measured at $(2.6, 2 \times 10^{-2})$ [34]. Considering the cement-sand mix ratio, the measured value for cement-concrete is consistent.

The clayed earth's relative permittivity and loss tangent are $(2.69,\ 2 \times 10^{-2})$. As a mixture of clay, sand, plus some air and moist, these values are in compliance with the mix ratio and the measured permittivity of clay $(4.4, 6 \times 10^{-2})$ [1] and sand (the dielectric characterization results may vary in the literature due to the origin of the studied materials).

For these three materials, the loss tangent poorly rises in the case of cement-concrete and Fermacell® although the relative permittivity notably increases. To understand, there is to remember that, for low loss tangent, the relative permittivity characterizes with what intensity the material polarizes with the applied electric field, while the loss tangent quantifies the delay between the field and the polarization vector. Following this definition, it can be said that this delay is not significantly modified by the presence of water for cement concrete.

3.3 Evaluation of the measurement uncertainties

According to [17], the measured complex relative permittivity of PVC is $(\epsilon_r, \tan(\delta))_{PVC} = (2.87, 0.9 \times 10^{-2})$. Our method, presented in part 2.2, leads to a value of $(\epsilon_r, \tan(\delta))_{PVC} = (2.97, 1.1 \times 10^{-2})$ which is in very good agreement.

Nevertheless, a Monte-Carlo numerical analysis was performed to estimate the systematic error from theoretical S-parameters data, knowing the uncertainty of the Vector Network Analyzer (VNA) from its datasheet: $\Delta|S_{ij}| \approx$ 0.2 dB and $\Delta arg(S_{ij}) \approx 1°$ in the conditions of use mentioned in 2.2. The module and phase uncertainties of each measured S-parameter are correlated. This last point is very important as four measurements of four S-parameters each have been performed consecutively for one extraction. Unfortunately, no correlation is given by the constructor between S-parameters of a same measurement and no correlation hypothesis have been formulated about this. On another side, the error on the same S-parameter for all four measurement has been considered equal because the measurements have been performed consecutively. Assuming this correlation hypothesis, the Monte-Carlo simulation evaluates the standard deviation to 0.08 for real relative permittivity and 2×10^{-2} for loss tangent.

4. Towards applications to the building sector: electromagnetic losses in walls

The previously presented dielectric permittivity characterizations are fundamental to the knowledge of electromagnetic behavior of construction materials over various RH conditions. It is thus possible to simulate the behavior of those materials in a realistic application, i.e. when used in walls and then to model the propagation channels of EM waves as a function of the ambient RH.

4.1 Monolayer wall: homogeneous material

The homogeneous monolayer wall studied here is $l = 10\ cm$ thick, surrounded by air and its behaviour is computed at a frequency $f = 1\ GHz$. From the measured complex permittivity $\bar{\epsilon}_{rMAT} = \varepsilon_r(1 - j\ \tan\delta)$, where ε_r is the real part of the dielectric permittivity and $\tan\delta$ the loss tangent of a material, the voltage reflection and transmission coefficients R and T of such a wall can be computed as follows [35]:

$$R = \frac{\sqrt{\bar{\epsilon}_{rAIR}} - \sqrt{\bar{\epsilon}_{rMAT}}}{\sqrt{\bar{\epsilon}_{rAIR}} + \sqrt{\bar{\epsilon}_{rMAT}}} \tag{5}$$

$$T = e^{-\frac{j\,2\pi f l}{c}\sqrt{\bar{\epsilon}_{rMAT}}} \tag{6}$$

The reflected power P_R and the transmitted power P_T (both normalized to an incident power of 1 W), can be expressed as in (7) and (8) [35].

$$P_R = \left|\frac{R(1 - T^2)}{1 - R^2T^2}\right|^2 \tag{7}$$

$$P_T = \left|\frac{T(1 - R^2)}{1 - R^2T^2}\right|^2 \tag{8}$$

Finally, the propagation losses or attenuation ATT can be calculated using (9) [35].

$$P_R + P_T + ATT = 1 \tag{9}$$

Those powers have been computed for all materials under test and for the three tested RH conditions (5%, 40% et 80%). The obtained results are presented in fig. 6.

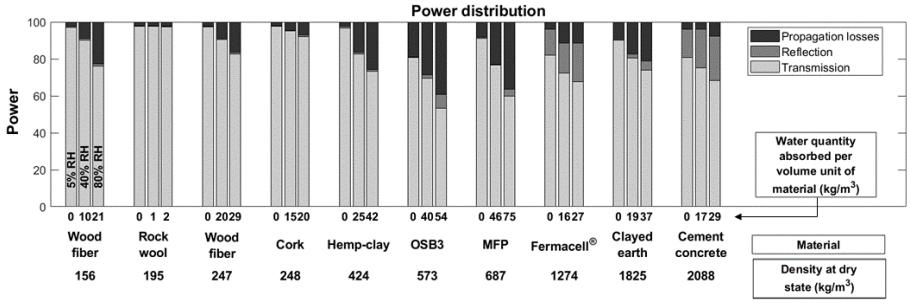

Fig. 6. Power distribution over propagation losses, reflection and transmission. The values were calculated choosing $L = 10\ cm$ and $f = 1\ GHz$.

At a fixed state, the reflection rate is significantly higher for materials of higher real relative permittivity like gypsum-fibers and cement concrete (as it was observed in 3.1). Indeed, a high permittivity implies more impedance disruption at the interface with air. For the other materials with a lower real permittivity, the propagation losses account for the largest part of the non-transmission. When the RH increases, the transmission rate shrinks as mainly the propagation losses rise with different sensitivity depending on the material. A correlation can be drawn between the propagation losses increase and the water quantity contained per volume unit of material in kg/m^3. The materials that transmit the least are gypsum-fibers and cement concrete (80,7 and 82,1 % of transmission for the considered thickness) at 5% RH and the wood panels OSB3 and MFP (53,3 and 59,8 %) at 80% RH. It is possible to say that at dry state, the mass effect is prominent in that it generally implies a higher real permittivity, thus a higher reflection rate and a lower transmission rate. Then, the quantity of water is the parameter responsible for the increase of the propagation losses leading to a shrink of the transmission rate.

4.2 Multilayer wall: a realistic case

The response of a realistic multilayer wall is studied here. The structure of the wall is described in Table 2.

Layer index	Thickness (mm)	Material	Comments
1	-	Air	Outside
2	22	Wood Panel (MFP)	Equivalent to wood cladding
3	18	Air	Air gap
4	220	Hemp-clay	Dense ecological insulator
5	15	Clayed earth + sand	Clayed earth coating
6	-	Air	Inside

Table. 2. Structure of the studied multilayer wall.

For a multilayer wall, the reflection and transmission coefficients R and T have to be computed step by step. Each layer i has its own transmission coefficient T_i which can be computed from (6). Each interface between two layers i et j has a reflection coefficient (conventionally defined for an incident wave coming from the outside) R_{ij} which ca be computed from (5). The air surrounding the wall on the outside and on the inside also has to be taken into account as two extra interfaces.

Finally, the whole set of coefficients constitutes the weights of a graph as shown on Fig. 7.

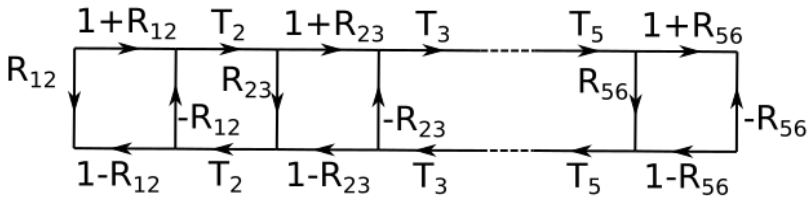

Fig. 7. Graph of a multilayer wall.

This graph is then reduced [35], and the global equivalent reflection and transmission coefficients can be computed leading to the determination of the power distribution between transmission, reflection and attenuation for each frequency point. Simulation results are shown on Figs. 8.a, 8.b and 8.c.

(a)

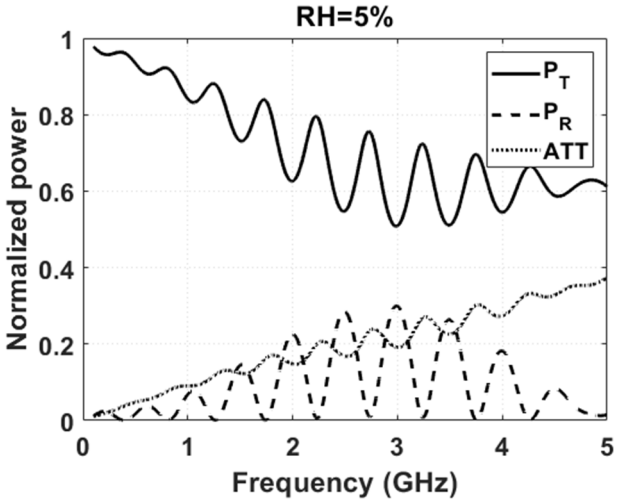
RH=5%
Normalized power
Frequency (GHz)
P_T
P_R
ATT
0
0.2
0.4
0.6
0.8
1
0
1
2
3
4
5

(b)

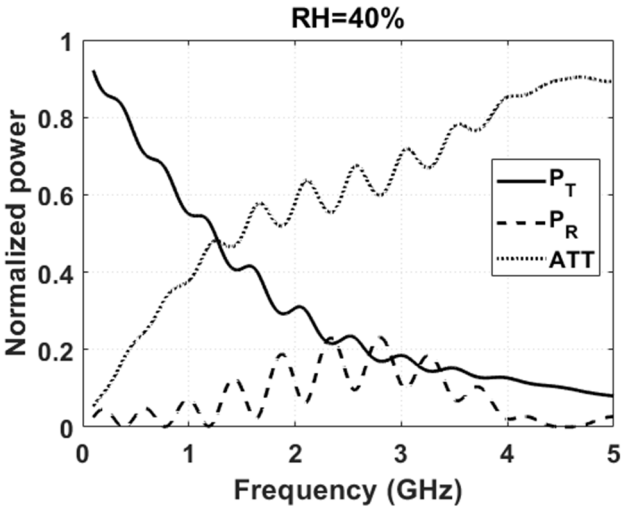
RH=40%
Normalized power
Frequency (GHz)
P_T
P_R
ATT
0
0.2
0.4
0.6
0.8
1
0
1
2
3
4
5

(c)

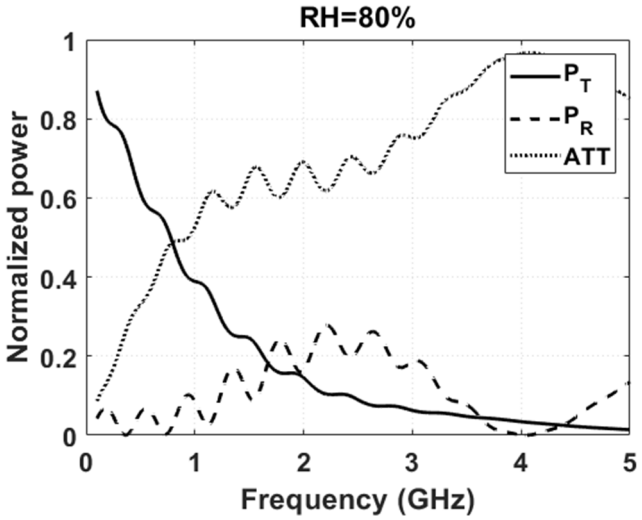

Fig. 8. Simulated frequency response of a multilayer wall depending on relative humidity (a) RH=5%, (b) RH=40%, (c) RH=80%.

As can be seen on fig. 8, the transmitted signal is drastically reduced with the increase of RH due to water absorption. This phenomenon becomes predominant when frequency is increased above a few gigahertz and when RH is greater than 40 %. Finally, the multilayer structure of the wall that alternates high and low real dielectric permittivities is responsible for the oscillations of the curves. Indeed, as soon as two plane permittivity interfaces face each other, the incident wave is infinitely reflected in the same way as the light is infinitely reflected by two opposite mirrors. This is known as a "Fabry–Pérot" cavity effect and implies the appearance of interference fringes.

5. Conclusion

Complex permittivity extraction results between 500 MHz and 2.5 GHz were given for some eco-materials used in the construction sector, at 5, 40 and 80 % RH. The water contents were measured by sample mass monitoring, which showed different water absorbing abilities. This study allowed to observe the variations of the dielectric properties of these particular materials according to the RH. The main tendency is that

both the relative permittivity and the dielectric losses increase with the RH. Two phenomena account for the loss of transmission: the impedance disruption at the interface with the material due to a high real relative permittivity on the one hand, and the water quantity contained in the material which increases the propagation losses on the other hand. The proposed study enables the modeling of an electromagnetic wave propagation channel at frequencies below 2.5 GHz depending on the relative humidity in a realistic building environment for any homogeneous or multilayer wall.

Acknowledgements

This work was funded by Lea Nature Foundation in the framework of the MAGBAT project, in collaboration between L'Association des Chanvriers en Circuits Courts, Ecopertica and Grenoble-Alpes University.

References

[1] N. R. Peplinski, F. T. Ulaby, M. C. Dobson, *« Dielectric properties of soils in the 0.3-1.3-GHz range »*, IEEE Transactions on Geoscience and Remote Sensing, vol. 33, no 3, p. 803–807, 1995.

[2] G. Villain, A. Ihamouten, X. Derobert, *« Determination of concrete water content by coupling electromagnetic methods: Coaxial/cylindrical transition line with capacitive probes »*, Ndt & E International, vol. 88, p. 59–70, 2017.

[3] A. Wahab, M. M. A. Aziz, A. R. M. Sam, K. Y. You, A. Q. Bhatti, K. A. Kassim, *« Review on microwave nondestructive testing techniques and its applications in concrete technology »*, Construction and Building Materials, vol. 209, p. 135–146, 2019.

[4] A. Joshaghani, M. Balapour, A. A. Ramezanianpour, *« Effect of controlled environmental conditions on mechanical, microstructural and durability properties of cement mortar »*, Construction and Building Materials, vol. 164, p. 134–149, 2018.

[5] J. O. Curtis, *« Moisture effects on the dielectric properties of soils »*, IEEE transactions on geoscience and remote sensing, vol. 39, no 1, p. 125–128, 2001.

[6] R. Olmi, M. Bini, A. Ignesti, C. Riminesi, *« Dielectric properties of wood from 2 to 3 GHz »*, Journal of Microwave Power and Electromagnetic Energy, vol. 35, no 3, p. 135–143, 2000.

[7] S. Trabelsi, S. O. Nelson, *« Free-space measurement of dielectric properties of cereal grain and oilseed at microwave frequencies »*, Measurement Science and Technology, vol. 14, no 5, p. 589, 2003.

[8] P. Xavier, A.-M. Belli-Riz., J.-Y. Frau, *« Caractérisation de l'atténuation radiofréquence de matériaux isolants naturels du bâtiment »*, in 11èmes Journées Caractérisation Microondes et Matériaux, Brest, France, 2010.

[9] V. Mandrić Radivojević, S. Rupčić, M. Srnović, G. Benšić, *« Measuring the Dielectric Constant of Paper Using a Parallel Plate Capacitor »*, International journal of electrical and computer engineering systems, vol. 9, no 1, p. 1–10, 2018.

[10] J. Krupka, *« Frequency domain complex permittivity measurements at microwave frequencies »*, Measurement Science and Technology, vol. 17, no 6, p. R55, 2006.

[11] E. Bourdel, D. Pasquet, P. Denorme, A. Roussel, *« Measurement of the moisture content with a cylindrical resonating cavity in TM/sub 010/mode »*, IEEE Transactions on instrumentation and measurement, vol. 49, no 5, p. 1023–1028, 2000.

[12] K.-P. Latti, M. Kettunen, J.-P. Strom, P. Silventoinen, *« A review of microstrip T-resonator method in determining the dielectric properties of printed circuit board materials »*, IEEE Transactions on Instrumentation and Measurement, vol. 56, no 5, p. 1845–1850, 2007.

[13] Amin Rida, Li Yang, Rushi Vyas, Swapan Bhattacharya, M. M. Tentzeris, *« Design and integration of inkjet-printed paper-based UHF components for RFID and ubiquitous sensing applications »*, in 2007 European Microwave Conference, 2007, p. 724-727, doi: 10.1109/EUMC.2007.4405294.

[14] J.-M. Heinola, K.-P. Latti, P. Silventoinen, J.-P. Strom, M. Kettunen, *« A new method to measure dielectric constant and dissipation factor of printed circuit board laminate material in function of temperature and frequency »*, in 9th

International Symposium on Advanced Packaging Materials: Processes, Properties and Interfaces (IEEE Cat. No. 04TH8742). 2004 Proceedings., 2004, p. 235–240.

[15] C. E. Kintner, *« Free-Space Measurements of Dielectrics and Three-Dimensional Periodic Metamaterials »*, 2017.

[16] V. V. Varadan, R. D. Hollinger, D. K. Ghodgaonkar, V. K. Varadan, *« Free-space, broadband measurements of high-temperature, complex dielectric properties at microwave frequencies »*, IEEE Transactions on Instrumentation and Measurement, vol. 40, no 5, p. 842–846, 1991.

[17] N. Tamyis, A. Ramli, D. Ghodgaonkar, *« Free space measurement of complex permittivity and complex permeability of magnetic materials using open circuit and short circuit method at microwave frequencies »*, in Student Conference on Research and Development, 2002, p. 394–398.

[18] H. Martens, J. Reedijk, H. Brom, *« Measurement of the complex dielectric constant down to helium temperatures. I. Reflection method from 1 MHz to 20 GHz using an open-ended coaxial line »*, Review of Scientific Instruments, vol. 71, no 2, p. 473–477, 2000.

[19] T. W. Athey, M. A. Stuchly, S. S. Stuchly, *« Measurement of radio frequency permittivity of biological tissues with an open-ended coaxial line: Part I »*, IEEE Transactions on Microwave Theory and Techniques, vol. 30, no 1, p. 82–86, 1982.

[20] S. S. Hasan, M. Sundaram, Y. Kang, M. K. Howlader, *« Measurement of dielectric properties of materials using transmission/reflection method with material filled transmission line »*, in 2005 IEEE Instrumentationand Measurement Technology Conference Proceedings, 2005, vol. 1, p. 72–77.

[21] W. Barry, *« A broad-band, automated, stripline technique for the simultaneous measurement of complex permittivity and permeability »*, IEEE Transactions on Microwave Theory and Techniques, vol. 34, no 1, p. 80–84, 1986.

[22] M. D. Janezic, J. A. Jargon, *« Complex permittivity determination from propagation constant measurements »*, IEEE microwave and guided wave letters, vol. 9, no 2, p. 76–78, 1999.

[34] P. M. Buff, J. Nath, M. B. Steer, *« Origin of the half-wavelength errors in microwave measurements using through–line calibrations »*, IEEE Transactions on Instrumentation and Measurement, vol. 56, no 5, p. 1610–1615, 2007.

[24] M. Degrave-Lemeurs, P. Glé, A. H. de Menibus, *« Acoustical properties of hemp concretes for buildings thermal insulation: Application to clay and lime binders »*, Construction and Building Materials, vol. 160, p. 462–474, 2018.

[25] V. Krotikov, *« Dielectric properties of dry soils »*, Izv. Vuzov. Radiophyz, vol. 5, no 6, p. 1057, 1962.

[26] A. B. Malkawi, H. Al-Mattarneh, B. E. Achara, B. S. Muhammed, M. F. Nuruddin, *« Dielectric properties for characterization of fly ash-based geopolymer binders »*, Construction and Building Materials, vol. 189, p. 19–32, 2018.

[27] C. Guers, F. Garet, P. Martinez, P. Xavier, T. Vuong, *« Impact of Water on the Dielectric Properties of Papers in the Radiofrequency Domain »*, in 2018 12th International Conference on Electromagnetic Wave Interaction with Water and Moist Substances (ISEMA), 2018, p. 1-9, doi: 10.1109/ISEMA.2018.8442303.

[28] F. T. Ulaby, M. A. El-Rayes, *« Microwave dielectric spectrum of vegetation-Part II: Dual-dispersion model »*, IEEE Transactions on Geoscience and Remote Sensing, no 5, p. 550–557, 1987.

[29] F. Sagnard, C. Vignat, V. Moncourtois, et E. Rolland, *« Détermination de la permittivité complexe de matériaux de construction dans le domaine microonde : comparaison des méthodes de Fresnel et d'ellipsométrie par réflexion »*, 2001.

[30] D. Ferreira, I. Cuiñas, R. F. Caldeirinha, T. R. Fernandes, *« A review on the electromagnetic characterisation of building materials at micro-and millimetre wave frequencies »*, in The 8th European Conference on Antennas and Propagation (EuCAP 2014), 2014, p. 145–149.

[31] C. Guers, *« Optimisation matériaux cellulosiques pour des applications en radiofréquences et térahertz »*, PhD Thesis, 2019.

[32] C. Guers, P. Xavier, F. Garet, Ph. Martinez, T.-P. Vuong, *« Impact de l'humidité sur les pertes des matériaux cellulosiques en RF »*, in 15èmes Journées de Caractérisation Microondes et Matériaux, Paris, France, 2018.

[33] D. J. Daniels, *« Ground penetrating radar »*, Encyclopedia of RF and Microwave Engineering, 2005.

485 [34] C. Matzler, *« Microwave permittivity of dry sand »*, IEEE Transactions on Geoscience and Remote Sensing, vol. 36, no 1, p. 317–319, 1998.

[35] D. M. Pozar, *« Microwave engineering »*, John Wiley & Sons, 2009.